ATMOSPHERIC CORRECTION, REFLECTANCE CALIBRATION AND BRDF CORRECTION FOR ADS40 IMAGE DATA

U. Beisl [a,*], J. Telaar [b], M. v. Schönermark [c]

[a] Leica-Geosystems AG, Heinrich-Wild-Strasse, 9435 Heerbrugg, Switzerland - Ulrich.Beisl@leica-geosystems.com
[b] now Astrium GmbH, Airbus-Allee 1, 28199 Bremen,Germany - Juergen.Telaar@astrium.eads.net
[c] IRS, Universität Stuttgart, Pfaffenwaldring 31, 70569 Stuttgart, Germany - Schoenermark@irs.uni-stuttgart.de

Commission VII, WG VII/1

KEY WORDS: Multispectral, Modelling, Aerial, Calibration, Land Use Mapping, Atmosphere, Radiometry, Correction

ABSTRACT:

A new radiometric workflow for ADS40 line scanner data has been developed and implemented. It includes now two additional atmospheric correction algorithms and an empirical BRDF correction. Both atmospheric correction algorithms are based on the radiation transfer equation by Kaufman and Sendra. The first method uses a dark target to determine the atmospheric haze. The key atmospheric quantities path radiance, upward and downward transmittance and spherical albedo are then calculated using a parametrisation for a specific atmosphere and aerosol type. The second method uses empirical approximations to calculate the gaseous absorption, Rayleigh and aerosol scattering. With the help of three free parameters (aerosol size, aerosol concentration, and single scattering albedo) the model can be adjusted to different atmospheres and aerosol types. The two methods have been verified with a set of ADS40 calibration flights over the same target with different visibilities. In-situ ground reflectance measurements of different targets were made. The calculated reflectance values were found to be in good agreement with the measured ones. The empirical correction of bidirectional reflection (BRDF) effects of the ground is performed using a modified Walthall model.

RÉSUMÉ:

Un nouveau flux de production radiométrique pour les données du capteur ADS40 a été développé et réalisé. Il consiste en deux algorithmes de correction atmosphérique et une correction BRDF empirique. Les deux algorithmes de correction atmosphérique sont basés sur l'équation de transfert de radiation par Kaufman et Sendra. La première méthode utilise une zone sombre pour déterminer la brume atmosphérique. Les principales quantités atmosphériques, (radiation diffuse de l'air, transmission ascendante, descendante et l'albédo sphérique) sont calculées en utilisant la parametrisation d'une atmosphère spécifique et d'un type d'aérosol. La deuxième méthode utilise des approximations empiriques pour calculer l'absorption gazeuse, la diffusion de Rayleigh ainsi que la diffusion de l'aérosol. Avec l'aide de trois paramètres libres (la dimension des particules de l'aérosol, la concentration de l'aérosol et l'albédo à diffusion simple) le modèle peut être adapté à différentes atmosphères et différents types d'aérosol. Les deux méthodes ont été véri-fiées avec un ensemble de vols de calibration ADS40 au même endroit et avec des visibilités différentes. Les mesures de réflectance ont été faites à endroits différents. On a constaté que les valeurs de réflectance calculées étaient en accord avec les mesures. La cor-rection empirique de réflexion bidirectionnelle (BRDF) de la terre est effectuée en utilisant le modèle de Walthall modifié.

KURZFASSUNG:

Ein neue radiometrische Prozessierungskette für ADS40 Zeilenscannerdaten wurde entwickelt und programmiert. Sie beinhaltet jetzt zwei zusätzliche Atmosphärenkorrekturalgorithmen und eine empirische BRDF-Korrektur. Beide Atmosphärenkorrekturalgorithmen setzen auf der Strahlungstransportgleichung von Kaufman and Sendra auf. Die erste Methode benutzt ein dunkles Objekt um die Stärke des atmosphärischen Dunsts zu bestimmen. Die entscheidenden atmosphärischen Größen, Luftlicht, aufwärts- und abwärtsge-richteter Transmissionsgrad und sphärische Albedo werden mittels einer Parametrisierung für eine bestimmte Atmosphäre und Aero-soltyp berechnet. Die zweite Methode benutzt empirische Näherungen um die Absorption durch die atmosphärischen Gase, die Rayleigh- und die Aerosolstreuung zu berechnen. Mittels dreier Parameter (Aerosolpartikelgröße, Aerosolkonzentration und Ein-fachstreualbedo) kann das Modell an verschiedene Atmosphären und Aerosoltypen angepasst werden. Die zwei Methoden wurden mit einer Reihe von ADS40 Testflügen über derselben Bodenfläche bei verschiedenen horizontalen Sichtweiten verifiziert. Gleich-zeitig wurden Messungen des Bodenreflexionsgrades von verschiedenen Objekten durchgeführt. Die berechneten Reflexionsgrade sind in guter Übereinstimmung mit den gemessenen Werten. Die empirische Korrektur der bidirektionalen Reflexion (BRDF) des Bodens wird mit Hilfe eines modifizierten Walthallmodells durchgeführt.

1. INTRODUCTION

For all passive Earth observation systems the presence of the atmosphere is a matter of concern - even for low flying airborne sensors like the ADS40. Airborne images show a wavelength, view and sun angle dependent haze background and contrast reduction. While those parameters are known during a flight campaign, the atmospheric composition is usually not measured,

---

* Corresponding author.

what makes it difficult to correct the images afterwards. Apart from a better contrast atmospherically corrected images can be more easily mosaicked and compared with each other for change detection. Atmospheric correction is also a prerequisite for quantitative remote sensing methods, which require images calibrated to ground reflectance.

For wide-angle sensors like the ADS40 the correction of the anisotropic reflectance (BRDF) of the ground is just as important for creating homogeneous images. Unfortunately the anisotropic reflectance is very much dependent on the subpixel surface structure of the ground which is also unknown.

So it is necessary to derive the necessary parameters for atmospheric and bidirectional reflectance correction from the image data itself.

For the case of atmospheric correction a number of all-purpose software packages exist (ATCOR, ATREM/TAFKAA, ACORN, FLAASH, etc). Those packages were developed for imaging spectrometers or multispectral sensors with relatively low spatial resolution and data volume. Therefore we decided to implement a set of rather simple but efficient algorithms to process the hundreds of Gigabytes of data of a typical high resolution image block. In order to find a compromise between a fast but insufficient contrast stretch and a time consuming radiation transfer model, methods from satellite remote sensing have been adapted to the specifics of airborne imagery and to the actual ADS40 spectral bands. The implementation follows the radiometric imaging chain proposed by (Beisl, 2006a).

A satellite version of the two methods has already been applied to MERIS data over land (Telaar and Schönermark, 2006).

2. ATMOSPHERIC EFFECTS

2.1 Empirical Models

Without any external data the atmospheric effects can only be determined using statistical methods working on the image data itself. Histograms of air- or spaceborne data show a band specific offset where the population starts. This is due to scattered light from below the sensor reaching the sensor field of view even if the ground reflectance is zero. This offset observed on a dark pixel is subtracted from each pixel to give the radiance at ground.

Simple Dark Pixel Subtraction: The original method as described above was proposed by (Chavez, 1975) for Landsat images. Here we assume a scan angle dependent offset and therefore investigate column specific histograms. The correction is done for each band separately.

Modified Chavez Method: In some cases where the image content was not a statistical mixture, an overcorrection was observed for the red and NIR bands (Chavez, 1988). Therefore Chavez proposed a prediction scheme which uses a $\lambda^{-\kappa}$ rule for the atmospherically scattered radiance. The exponent κ ranges from 4 for a clear Rayleigh-type atmosphere to 0.5 for a very hazy atmosphere. Since the blue band offset shows the largest atmospheric effect this is supposed to be the most accurate value. The calibrated radiance value of this offset allows to decide the κ value. The larger the offset the hazier the atmosphere. The κ decision rule has to be flying height dependent. With the $\lambda^{-\kappa}$ rule the offset values for the green, red

and NIR band are calculated. Examples have been shown already in (Beisl, 2006a).

2.2 Physical Models

For large homogeneous surfaces the measured radiance at the sensor is (Kaufman and Sendra, 1988, Fraser et al., 1992).

$$L_m = L_0 + \frac{\rho S T_{down} T_{up}}{\pi(1 - s\rho)} \qquad (1)$$

where L_m = measured at-sensor radiance
L_0 = path radiance for zero surface reflectance
ρ = surface reflectance
S = mean solar spectral irradiance
T_{down} = total downward transmittance from top of the atmosphere (TOA) to the ground
T_{up} = total upward transmittance from ground to sensor
s = spherical albedo of the atmosphere, i.e. the fraction of the upward radiance which is backscattered by the atmosphere

This equation can be solved for the reflectance ρ

$$\rho = \frac{f}{1 + sf} \qquad (2)$$

where $\qquad f \equiv \frac{\pi(L_m - L_0)}{S T_{down} T_{up}} \qquad$ **(3)**

The term $1 - s\rho$ takes into account the multiple scattering from the surrounding area. For a non-uniform surface the target reflectance ρ has to replaced by an average reflectance $\overline{\rho}$ of the surrounding area (Tanré et al., 1981). For a darker (brighter) surrounding area this leads to a lower (higher) at-sensor radiance (adjacency effect, Dave 1980).

$$L_m = L_0 + \frac{\rho S T_{down} T_{up}}{\pi(1 - s\overline{\rho})} \qquad (4)$$

The reflectance then calculates as

$$\rho = \frac{\pi(L_m - L_0)}{S T_{down} T_{up}}(1 - s\overline{\rho}) \qquad (5)$$

If we know $\overline{\rho}$ this takes up the form of an affine function of the measured radiance L_m with correction constants A and B.

$$\rho = A L_m + B \qquad (6)$$

Actually $\overline{\rho}$ is an integral of the reflectances weighted by the distance from the target and depending on the view angle and on the Rayleigh and aerosol contributions to the transmittance. (Richter, 1996) gives an effective range of 500 m to 1000 m for airborne images, and for flying heights H less than 1 km, the effective range is H/2. Calculating the integral causes an

immense computation effort, so (Richter and Schläpfer, 2002) use a value of 0.15 for $\overline{\rho}$.

In our case, we will use a resampled image of minification level 32 to calculate a low resolution image with eqn. (2), thereby neglecting the adjacency effect for the already large pixels. Interpolation then gives an estimate of $\overline{\rho}$ for each high resolution pixel.

The mean solar irradiance S at solar zenith angle θ_i is calculated from the solar constant S_0 and the ratio of Earth-Sun distance a to mean Earth-Sun distance r.

$$S = S_0 (a/r)^2 \cos \theta_i \qquad (7)$$

The measured at-sensor radiances L_m can be obtained from the ADS40 data as described in (Beisl, 2006b). Now we need a method to calculate the unknown quantities L_0, T_{down}, T_{up}, and s.

Ångström Method: This method provides a way of calculating the quantities L_0, T_{down}, T_{up}, and s using the following assumptions: clear atmosphere with rural aerosols and a horizontal visibility above 11 km. The approximations follow (Iqbal, 1983) and have three free parameters: aerosol size α, aerosol concentration β, and single scattering albedo ω_0. For brevity only an outline is given here.
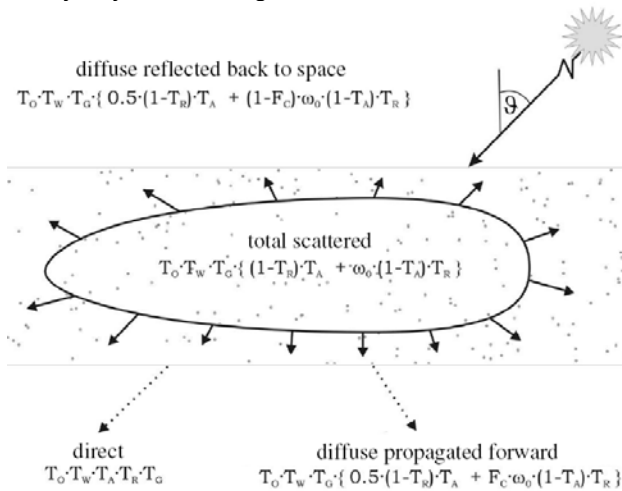
Figure 1. Direct and scattered components of the radiation (Iqbal, 1983)

For calculating the downward transmittance T_{down} the direct T_{dir} and the diffuse T_{dif} contribution have to be considered according to **Figure 1**:

$$T_{dir} = T_R T_O T_G T_W T_A \qquad (8)$$

The Rayleigh contribution T_R only depends on wavelength λ and solar zenith angle and is described by the formula from (Bucholtz, 1995). The gaseous absorption T_G in the ADS40 channels can be neglected except the ozone absorption T_O, where the values of Leckner quoted by (Iqbal, 1983) are used. The water absorption T_W is only relevant in the near Infrared (NIR), where we use again (Iqbal, 1983). The aerosol contribution T_A is described by the Ångström turbidity formula and introduces two parameters α and β, which determine the extinction coefficient k_A.

$$k_A = \beta \cdot \lambda^{-\alpha} \qquad (9)$$

The wavelength exponent α is a measure for the aerosol size distribution. The Ångström turbidity coefficient β describes the aerosol concentration. The values range from $\alpha = 1.3$ for small particles to $\alpha = 0.1$ for large particles and $\beta = 0.1$ for clear atmosphere to $\beta = 0.4$ for hazy atmosphere.

The diffuse forward transmission T_{dif} contains the parameter ω_0 which is set to 0.9 for rural and to 0.6 for urban aerosols.

$$T_{dif} = T_O T_G T_W \left((1 - T_R) \frac{T_A}{2} + F_C \omega_0 (1 - T_A) T_R \right) \quad (10)$$

Turning **Figure 1** upside down we can calculate the upward transmittance T_{up} for an illumination coming from the ground. The spherical albedo s is the diffuse reflected part of this process. Since the multiple scattering is only a second order effect, we approximate the incidence zenith angle for calculating T_W, T_R, T_O, T_A, and F_C by 60° and use a relative air mass of 1.9 .

$$s = T_O T_G T_W (0.5(1 - T_R) T_A + (1 - F_C) \omega_0 (1 - T_A) T_R) \qquad (11)$$

For calculating the path radiance for zero ground reflectance L_0 we also consider two contributions. The direct part originates from the diffuse reflected part between ground and sensor of the direct irradiance at sensor level. The diffuse part comes from the diffuse reflected part between ground and sensor of the diffuse forward scattered irradiance at sensor level. Again the incidence zenith angle of the diffuse irradiance is approximated by 60°.

Modified Song-Lu-Wesely Method: For the case of a satellite sensor (AVHRR) (Song et al., 2003) use a linear parametrisation in atmospheric reflectance δ_0, view zenith angle θ_r and sun zenith angle θ_i to calculate L_0, T_{down}, T_{up}, and s. Since we are dealing with an airborne sensor we have the additional variables ground level H and flight altitude over ground h. The atmospheric reflectance for nadir sun and nadir view zenith angle δ_0 itself is parametrised ($a_1 \ldots a_4$) and calculated from the measurement of the atmospheric reflectance δ above a dark pixel.

$$\delta_0 = \delta_0 (\delta, a_1 \cdots a_4, \theta_r, \theta_i) \qquad (12)$$

The atmospheric reflectance δ is defined here as the difference of a pseudo reflectance α and the ground reflectance ρ.

$$\alpha \equiv \frac{\pi \, L_m}{S} \qquad (13)$$

$$\delta \equiv \alpha - \rho \qquad (14)$$

For a dark water pixel we can model the reflectance ρ with the Fresnel reflectance of water = 2 %. It turned out that it is a good approximation to use this value also for dark dense vegetation or a grey shadow pixel. Then δ_0 can be calculated for this pixel, which is observed at a view zenith angle θ_r and a sun zenith

angle θ_i . This δ_0 is used to calculate L_0, T_{down}, T_{up}, and s for all image locations.

$$L_0 = L_0(b_1 \cdots b_7, \theta_r, \theta_i, \delta_0, h, H) \qquad (15)$$

$$T_{down} = T_{down}(c_1 \cdots c_6, \theta_i, \delta_0, h, H) \qquad (16)$$

$$T_{up} = T_{up}(d_1 \cdots d_3, \theta_r, \delta_0) \qquad (17)$$

$$s = s(e_1 \cdots e_6, \delta_0, h, H) \qquad (18)$$

The parameters ($a_1...a_4$, $b_1...b_7$, $c_1...c_6$, $d_1...d_3$, $e_1...e_6$) were determined separately for each band using a multilinear regression with simulated atmospheric data. The data were calculated in a range of 500 m to 9000 m for the flying height over ground, 0 m to 6000 m for the ground elevation, 7 km to 100 km for the visibility, 0° to 60° for the sun zenith angle, and 0° to 35° for the view zenith angle.

Figure (2) shows the linear correlation coefficients r^2 for the different quantities. Due to the large number of parameters we obtain a very high correlation above 0.992. The decrease in correlation for s in the NIR band is of no significance, since the s-dependence is a second order effect.
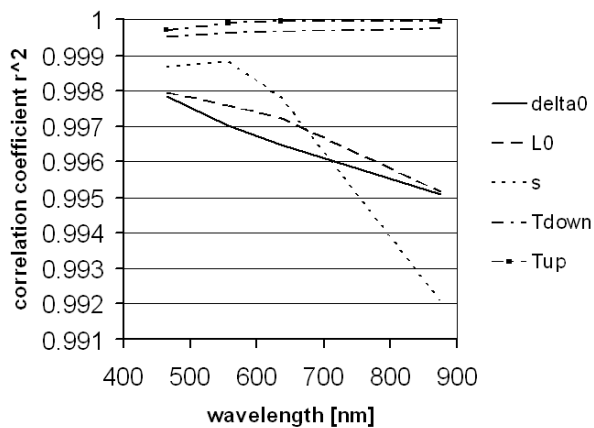
Figure 2. Correlation coefficients for the parametrised quantities δ0, L0, Tdown, Tup, and s for the ADS40 bands B, G, R, NIR.

Model sensitivity: Neglecting the multiple reflection term sρ in eqn. (5) the error in reflectance $\Delta\rho$ caused by the path radiance uncertainty ΔL_0 is

$$\Delta\rho = \frac{\partial\rho}{\partial L_0}\Delta L_0 \approx -\frac{\pi}{T_{down}T_{up}S}\Delta L_0 \qquad (19)$$

So in order to keep the output reflectance error small the path radiance error has to be kept as small as possible. This requires a careful selection of the dark pixel. Eqn. (19) also shows that the absolute reflectance error becomes larger for smaller transmission, i.e. for a hazy atmosphere.

3. BIDIRECTIONAL EFFECTS

As already presented in (Beisl, 2004) the Walthall model (Walthall et al., 1985, Nilson and Kuusk, 1989), which is

extended by a hot spot term D, can be used for correcting the bidirectional effects. Eqn. (20) is a linear function of its free parameters and can be easily inverted using a least squares regression.

$$\rho(\theta_i, \theta_r, \varphi) = \\ a\theta_i^2\theta_r^2 + b(\theta_i^2 + \theta_r^2) + c\theta_i\theta_r \cos\varphi + dD + e \qquad (20)$$

where
ρ = reflectance factor
θ_i = incident illumination zenith angle
θ_r = reflection view zenith angle
φ = relative azimuth angle
D = hot spot term
a, b, c, d, e = free parameters

$$D = \sqrt{\tan^2\theta_i + \tan^2\theta_r - 2\tan\theta_i \tan\theta_r \cos\varphi} \qquad (21)$$

The samples for model inversion can be retrieved by calculating column averages of the total image as described in (Beisl, 2004), since a column in a line scanner image represents a line of constant view angle. The relative shape of the modelling is then used for a multiplicative correction.

For a good inversion quality, i.e. for all images matching together in the mosaic, it is recommended to merge the statistics from each image together and perform a simultaneous correction (Beisl, 2002). This will also improve the correction of images with inhomogeneous statistics.

4. DATA AND RESULTS

In order to verify the two new atmospheric correction algorithms (Ångström method and Modified Song-Lu-Wesely Method) ground reflectance measurements have been carried out in the center area of the test flight region. The test flight pattern was a double cross strip at two different flying heights (1500 m and 2500 m above ground). In total four image blocks with four different atmospheres (visibility 10 km, 20 km, 30 km, and 40 km) were tested in the same area.

Figures 3 and 5 show the correction results for two different horizontal visibilities (10 km and 20 km) which is an empirical measure for the aerosol content. The uncorrected pseudo reflectance shows a blue hue due to Rayleigh scattering. The modified Song-Lu-Wesely method and the Ångström method correct this phenomenon, the latter works slightly stronger. It can also be seen that a BRDF correction is still necessary to homogenize the image.

Figures 4 and 6 show a grass target observed from two directions and two flying heights on two days with different visibilities. Already the pseudo reflectance shows a stable reflectance result. The modified Song-Lu-Wesely method and the Ångström method correct the blue hue and give a more accurate value for the NIR reflectance.

For an asphalt target (reflectance ≈ 0.15, not shown here) the results of pseudo reflectance, modified Song-Lu-Wesely method and the Ångström method are also constant with flying height, visibility and flight direction. The discrepancy from the measured ground reflectance is at most 0.03. The blue hue is removed and the NIR value is unchanged.

Figure 3. April 19, 2007, 09:54 h, nadir, flying height 2500 m above ground, visibility 10 km, without BRDF correction (left to right): uncorrected pseudo reflectance, modified Song-Lu-Wesely method, Ångström method.

Figure 5. March 28, 2007, 09:58 h, nadir, flying height 2500 m above ground, visibility 20 km, without BRDF correction (left to right): uncorrected pseudo reflectance, modified Song-Lu-Wesely method, Ångström method.
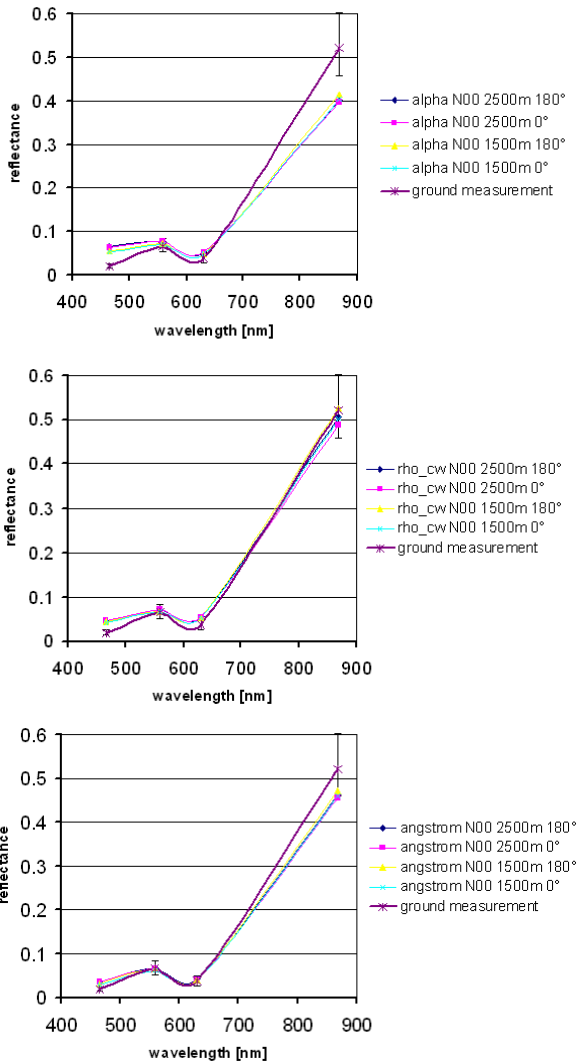
Figure 4. April 19, 2007, nadir view, grass target on 4 images in opposite direction (heading 0° and 180°) and flying height 1500 m and 2500 m above ground, visibility 10 km (top to bottom): uncorrected pseudo reflectance, modified Song-Lu-Wesely method, Ångström method.
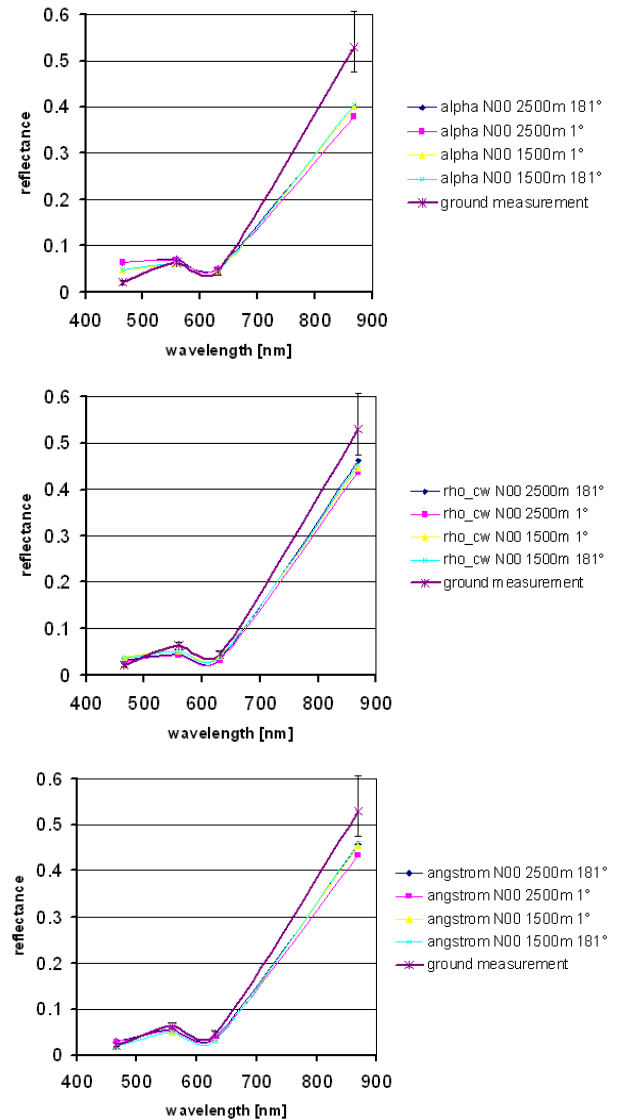
Figure 6. March 28, 2007, nadir view, grass target on 4 images in opposite directions (heading 1° and 181°) and flying height 1500 m and 2500 m above ground, visibility 20 km (top to bottom): uncorrected pseudo reflectance, modified Song-Lu-Wesely method, Ångström method.

5. CONCLUSIONS

In this paper we have shown two new methods for the correction of atmospheric and BRDF effects in ADS40 images which will be implemented in the new ADS40 radiometric imaging chain. In contrast to the existing atmospheric correction methods in GPro which produce a radiance output, the new methods divide out the effect of solar irradiance and produce reflectance which is a surface property. A further advantage of reflectances is that the image dynamics of the different images in an image block is adjusted to match together.

Both models have the free variables flying and ground height as well as view zenith and sun zenith angle. For a fast correction the two heights and the sun zenith angle can be set constant. The remaining view angle dependence results in a look-up-table of correction constants A and B as defined in eqn. (6). The ADS40 line scanner geometry allows a simple line by line correction.

The BRDF correction reduces the intrinsic image gradients, without removing image fluctuations and is the final step before the image mosaicking. Remaining seams can then be removed with conventional feathering. This is a step towards an automatic generation of huge seamless maps.

6. OUTLOOK

In the current implementation the dark pixel value is determined for each band separately. Using the geometric sensor model a correlation of different bands can improve the selection result and lead to a spectral classification.

For a better support of quantitative methods in remote sensing, a step to a more accurate correction will be the integration of topographic effects in atmospheric correction. The resulting irradiance on the ground depends on slope and aspect of the terrain, as well as the sky view factor for each point, i.e. the fraction of the sky that is visible from the given point. This needs integrating the geometric sensor model and an elevation model in the radiometric correction and includes also non-local effects, like shadowing from distant points.

Finally a class specific BRDF modelling would reflect the individual differences in BRDF behaviour of ground surfaces. This would assist a later classification and time series analysis.

REFERENCES

Beisl, U., 2002. Simultaneous correction of bidirectional effects in line scanner images of rural areas. *Proc. 9th International Symposium in Remote Sensing (SPIE)*, Agia Pelagia, Crete,10 p.

Beisl, U., and Woodhouse, N., 2004. Correction of atmospheric and bidirectional effects in multispectral ADS40 images for mapping purposes. *Proc. XXth Congress of the ISPRS,* Istanbul, Turkey, 12-23 July, 5 p.

Beisl, U., Woodhouse, N., and Lu, S., 2006a. Radiometric processing scheme for multispectral ADS40 data for mapping purposes. *Proc. Ann. Conf. ASPRS,* Reno, USA, 1-5 May, 9 p.

Beisl, U., 2006b. Absolute spectroradiometric calibration of the ADS40 sensor. *Proc. of the ISPRS Commission I Symposium "From Sensors to Imagery",* Paris – Marne-la-Vallée, France, 3-6 July, 5 p.

Bucholtz, A, 1995. Rayleigh-scattering calculations for the terrestrial atmosphere, *Appl. Opt.*, 34(15), pp. 2765-2773.

Chavez, P. S., Jr., 1975. Atmospheric, solar, and MTF corrections for ERTS digital imagery. *Proc. Am. Soc. Photogrammetry*, Fall Technical Meeting, Phoenix, AZ, p. 69.

Chavez, P. S., Jr., 1988. An improved dark-object subtraction technique for atmospheric scattering correction of multispectral data. *Remote Sens. Environ.*, 24, pp. 459-479.

Dave, J. V., 1980. Effect of atmospheric conditions on remote sensing of a surface non-homogeneity. *Photogramm. Eng. Remote Sens.*, 46(9), pp. 1173-1180.

Fraser, R. S., Ferrare, R. A., Kaufman, Y. J., Markham, B. L., and Mattoo, S., 1992. Algorithm for atmospheric corrections of aircraft and satellite imagery. *Int. J. Remote Sensing*, 13(3), pp. 541-557.

Iqbal M., 1983. *An introduction to solar radiation*. Academic Press Canada.

Kaufman, J. Y., and Sendra, C, 1988. Algorithm for automatic atmospheric corrections to visible and near-IR satellite imagery, *Int. J. Remote Sensing*, 9(8), pp. 1357 – 1381.

Nilson, T., and Kuusk, A., 1989. A reflectance model for the homogeneous plant canopy and its inversion. *Remote Sens. Environ.*, 27, pp. 157-167.

Richter, R., 1996. Atmospheric correction of DAIS hyperspectral image data. *Computers & Geosciences*, 22(7), pp. 785-793.

Richter, R., Schläpfer, D., 2002. Geo-atmospheric processing of airborne imaging spectrometry data. Part 2: atmospheric / topographic correction. *Int. J. Remote Sensing*, 23(13), pp. 2631-2649.

Song, J., Lu, D., and Weseley, M. L., 2003. A simplified atmospheric correction procedure for the normalized difference vegetation index. *Photogramm. Eng. Remote Sens.*, 69(5), pp. 521-528.

Tanré, D., Herman, M., and Deschamps, P. Y., 1981. Influence of the background contribution upon space measurements of ground reflectance, *Appl. Opt.*, 20, pp. 3676-3684.

Telaar, J., and Schönermark, M. v., 2006. Comparison of three simplified algorithms for atmospheric corrections of MERIS data over land. Proc. Atmospheric Science Conference, ESA ESRIN, Frascati, Italien, 8.-12. May, 6 p.

Walthall, C. L., Norman, J. M., Welles, J. M., Campbell, G., and Blad, B. L., 1985. Simple equation to approximate the bidirectional reflectance from vegetative canopies and bare soil surfaces. *Appl. Opt.*, 24(3), pp. 383-387.